

Review

Formidable Challenges in Additive Manufacturing of Solid Oxide Electrolyzers (SOECs) and Solid Oxide Fuel Cells (SOFCs) for Electrolytic Hydrogen Economy toward Global Decarbonization

Majid Minary-Jolandan 

Department of Mechanical Engineering, The University of Texas at Dallas, Richardson, TX 75080, USA; majid.minary@utdallas.edu

Abstract: Solid oxide electrolysis cells (SOECs) and solid oxide fuel cells (SOFCs) are the leading high-temperature devices to realize the global “Hydrogen Economy”. These devices are inherently multi-material (ceramic and cermets). They have multi-scale, multilayer configurations (a few microns to hundreds of microns) and different morphology (porosity and densification) requirements for each layer. Adjacent layers should exhibit chemical and thermal compatibility and high-temperature mechanical stability. Added to that is the need to stack many cells to produce reasonable power. The most critical barriers to widespread global adoption of these devices have been their high cost and issues with their reliability and durability. Given their complex structure and stringent requirements, additive manufacturing (AM) has been proposed as a possible technological path to enable the low-cost production of durable devices to achieve economies of scale. However, currently, there is no single AM technology capable of 3D printing these devices at the complete cell level or, even more difficult, at the stack level. This article provides an overview of challenges that must be overcome for AM to be a viable path for the manufacturing of SOECs and SOFCs. A list of recommendations is provided to facilitate such efforts.

Keywords: SOEC; SOFC; hydrogen economy; renewable energy; decarbonization; additive manufacturing; market competitiveness; scale-up and high-volume manufacturing



Citation: Minary-Jolandan, M. Formidable Challenges in Additive Manufacturing of Solid Oxide Electrolyzers (SOECs) and Solid Oxide Fuel Cells (SOFCs) for Electrolytic Hydrogen Economy toward Global Decarbonization. *Ceramics* **2022**, *5*, 761–779. <https://doi.org/10.3390/ceramics5040055>

Academic Editor: Narottam P. Bansal

Received: 21 September 2022

Accepted: 12 October 2022

Published: 14 October 2022

Publisher’s Note: MDPI stays neutral with regard to jurisdictional claims in published maps and institutional affiliations.



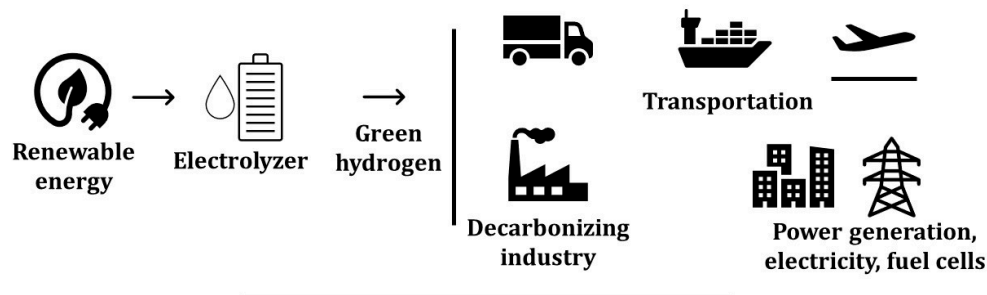
Copyright: © 2022 by the author. Licensee MDPI, Basel, Switzerland. This article is an open access article distributed under the terms and conditions of the Creative Commons Attribution (CC BY) license (<https://creativecommons.org/licenses/by/4.0/>).

1. Introduction

Hydrogen, as an important chemical feedstock in the global economy, has growing demands in transportation, steel production, power generation, and load balancing in grid services. Recently, there has been a significant global investment in the “Hydrogen Economy”, which in turn will advance the manufacturing and recycling of clean hydrogen technologies. For example, in the United States, the mission of the Department of Energy’s “Hydrogen Shot” is to reach USD 1 per 1 kg in 1 decade (“1 1 1”) for hydrogen. Sectors such as long-distance transport via heavy- and medium-duty vehicles, high-temperature heat, energy storage, and synthetic fuels for air and marine transport are among the energy-intensive and difficult sectors to decarbonize. Hydrogen has been proposed as a key energy option for the decarbonization of these sectors (Figure 1).

Hydrogen is the simplest element on earth; however, it does not typically exist by itself in nature. It must be produced through chemical reactions from compounds that contain it. Currently, the majority (~95%) of the world’s hydrogen is produced by steam methane reforming (SMR) that releases the greenhouse gas CO₂. The electrolytic hydrogen (without any pollution) is more expensive compared to hydrogen produced using the SMR process [1]. Today’s hydrogen market is approximately 10 million metric tons per year (MMT/year) in the U.S. and 65–100 MMT/year globally. However, only approximately 2% of total global hydrogen production is generated via electrolysis. The electrolytic hydrogen

market could grow substantially to at least 100 MMT/year by 2050 to meet potential future demands and help difficult-to-decarbonize sectors. In order to meet this market size, the U.S. electrolyzer capacity will likely have to increase from 0.17 gigawatts (GW) today to up to 1000 GW in 2050—or 20% compound annual growth from 2021 to 2050 with an annual manufacturing requirement of over 100 GW/year [2]. In addition, over 50 GW of domestic fuel cell capacity is required in the decarbonization scenario, with an annual manufacturing requirement of over 3 GW/year. Investments in manufacturing and process development and increasing production scale and industrialization will reduce the cost of electrolytic hydrogen.



Critical barriers to widespread applications: High cost and durability/reliability issues

Figure 1. Roles of fuel cells and electrolyzers in the hydrogen economy.

SOFCs and SOECs are considered among the electrochemical energy storage and conversion devices that are essential for the global rollout of a hydrogen economy. SOECs are energy storage units that produce storable hydrogen from electricity and water (electrolysis of water), electrolyze CO₂ to produce CO and oxygen, or even co-electrolyze water and CO₂ to produce syngas (CO + H₂) and oxygen [3]. High-temperature steam electrolyzers use both electricity (preferably renewable) and heat (preferably waste heat or a low-cost thermal energy generator such as a nuclear reactor) because they operate with steam. SOFCs convert the chemical energy stored in a fuel (H₂, CO, CH₄, etc.) to electricity directly through an electrochemical reaction (by oxidizing a fuel). SOFCs are often composed of approximately 40–60 individual cells that produce nearly 25 W per cell, interconnected into a single module [4].

The key barriers to the existing technologies are fabrication time and cost, quality assurance and quality control, as well as stack durability. Despite their high efficiency, the global market rollout of these devices is currently short of economies of scale. The benefits of the hydrogen economy will be best played out when it is deployed at scale and across multiple applications. However, the high cost of these devices compared to alternative energy systems is the single most important factor hindering their widespread applications.

SOFCs and SOECs and their stacks are geometrically complex, inherently multi-material, and multilayer devices. The cells are made of thin active elements (~10–50 μm electrolyte and ~50–300 μm anode and cathode) with different compositions and microstructures (porous anode and cathode and dense electrolyte). More than a hundred steps could be involved in the traditional manufacturing process of a complete stack, including tape-casting, screen printing, slip-casting, slurry spraying, spray pyrolysis, dip-coating, thin film deposition, chemical infiltration and ex-solution for catalysts, and laser cutting of the fabricated tapes, punching, laminating, stacking, and firing/sintering [5–7]. Many steps, with most requiring manual inputs and multiple joints and seals, result in low reliability, durability and reproducibility, high cost, and a long time to market (Figure 2). For the global-scale adaptation of these devices, manufacturing technologies are needed that reduce the number of cell components in a stack, lower processing temperature, reduce the number of processing steps, and shorten the overall processing time. These improvements may result in an increase in throughput and lower-cost production at scale [2].

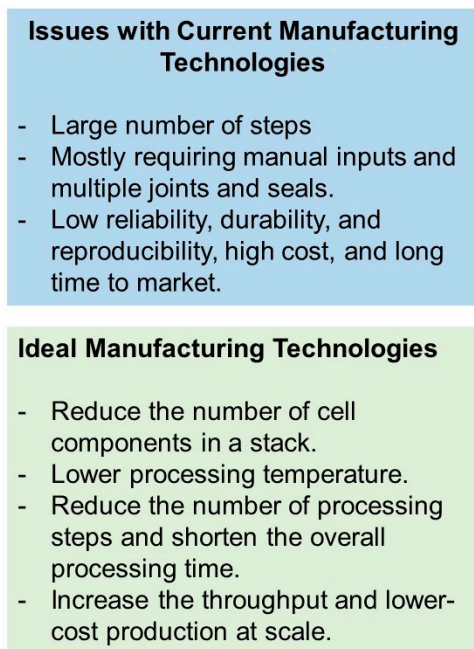


Figure 2. Issues with current manufacturing technologies for production SOFCs and SOECs and attributes of ideal manufacturing technologies for these devices.

Development or application of suitable additive manufacturing (AM) technologies has the potential to lower the manufacturing cost, decrease waste of often expensive raw materials, provide use of more environmentally friendly materials and processing methods, and use fewer solvents. AM technologies may reduce the number of steps and result in more durable and reliable devices. Another advantage of AM technologies may be the augmentation of the design space for more efficient devices, such as enabling complex geometries beyond planar and tubular ones or enhancing surface area for electrochemical reaction sites and enhancing specific power [8]. Thermomechanical modeling of 3D manufactured electrodes for SOFCs, and rational design of 3D manufactured composite electrodes point to the benefits of 3D printing for performance improvement if certain design criteria are considered [9,10].

Given the largely nascent nature of the SOEC and SOFC industries, there are limited data on supply chain needs and constraints [1]. High-volume production of these energy devices requires building multi-industry supply chains to support components, materials, and equipment [2]. Some cell materials and components, such as interconnects, may face supply chain issues, considering that interconnects are more prone to degradation (cracking, delamination, and coating pinholes). AM allows for distributed manufacturing that can elevate some of the concerns in the supply chain.

The goal of this article is to provide a brief overview of challenges that should be overcome for AM to be a viable path to produce these energy devices. The aim is to help identify current bottlenecks and the required R&D strategies that will result in maturation of these technologies and the at-scale production of these devices. A list of recommendations is provided to facilitate such efforts. This article does not discuss various AM processes and their working principles in depth. Readers are encouraged to refer to more focused reviews on various AM processes [5,11–16].

2. SOECs and SOFCs Components and Requirements

At the basic level, these electrochemical devices are made of an electrolyte and two electrodes (anode and cathode). Interconnects and sealing materials are also required for complete cells and stacks. The electrolyte and the electrodes should have a proper thickness to reduce electric and diffusion resistance. The microstructure and, to some extent, the thickness of the functional materials in these devices primarily govern the

device's performance [17]. The electrolyte is a pure ceramic, while the anode and cathode are ceramic-metal composites (cermet). A dense, thin electrolyte is required to separate oxidation gases from fuel gases. When the cell is electrode-supported, the thickness of the electrolyte can be substantially reduced (to a few microns), which results in a significant reduction in the overall ohmic resistance of the cell. Thinner electrolyte, however, limits the number of 3D printing technologies that are applicable. Cathode and anode are a mixture of electrolyte and electrode materials, which is preferred for reduced polarization and expansion of the triple phase boundaries (TPBs).

ZrO₂ doped by Yttrium (Y) or Scandia (Sc) are conductors of oxygen ions above 800 °C. Currently, yttria-stabilized zirconia (YSZ) is the state-of-the-art electrolyte material for SOFCs and SOECs. YSZ can be generally sintered in the temperature range of 1300–1500 °C [18]. Sc-stabilized zirconia (ScSZ) and gadolinium-doped ceria (GDC) have also been used as electrolytes [19]. The electrolyte must be sufficiently dense to avoid leakage of the fuel/oxidant gases to the electrodes and reduce the resistance to oxygen ion diffusion in the electrolyte. The electronic conductivity of the electrolyte should be low to prevent losses due to leakage current. The density of the electrolyte, which is related to porosity, plays an important role in its electrical conductivity. Flaws, pinholes, and other defects in the electrolyte can drastically reduce the electrochemical performance of the cell. The sintering step of the electrolyte ceramic is, therefore, vital.

Nickel-YSZ (Ni-YSZ) cermet is used as the anode in SOFC and the cathode in SOEC (considered fuel electrode in both devices). YSZ ceramic in this cermet provides ionic conductivity and structural support, while Ni functions as the catalyst and electronic conductor [20]. The cathode in SOFC and anode in SOEC (or the oxygen electrode) can be made of mixed conductors such as lanthanum-strontium cobalt ferrite (LSCF) or lanthanum-strontium cobaltite (LSC). LSCF is a mixed ion-electronic conductor capable of fast oxygen ion and electron conduction. It promotes oxygen reduction reaction as a highly active catalyst. Strontium (Sr)-doped LaMnO₃ (LSM) in a cermet with YSZ may be used for less demanding applications. LSM has good compatibility and low chemical reactivity with YSZ and a similar coefficient of thermal expansion (CTE) to YSZ. In this case, LSM provides electronic conduction and catalytic function, while YSZ is the structural component and provides ionic conduction. In some designs, a buffer layer of gadolinium doped ceria (GDC) is used between the electrolyte and the LSCF cathode. In order to prevent a reaction between the oxygen electrode materials and YSZ, a thin (0.1 to 5 µm) layer of GDC may also be utilized [3].

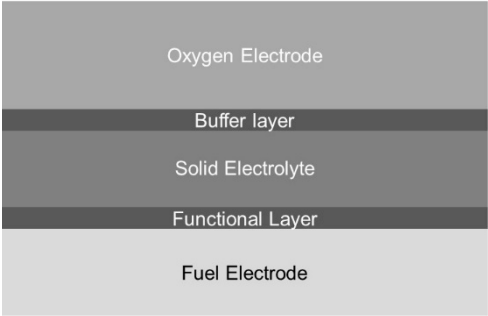
In terms of recycling and circular economy in SOFCs and SOECs, Ni and Lanthanum elements are considered among the materials with environmental burdens. These burdens can be remediated (estimated ~70%) with recycling and considerations of the circular economy approach [21].

Cathode and anode are porous, electrically conductive, and should possess high catalytic activities for fuel oxidation and oxygen reduction, which requires a high density of reactive electrochemical sites, or triple phase boundaries, TPBs. An electrochemical reaction occurs at the TPBs, where electrons, ions, and reactants meet. Porosity is required to provide pathways for mass transport, i.e., diffusion of gaseous fuels and byproducts. The polarization in each electrode includes ohmic, activation, and concentration polarizations, which should be optimized for the overall minimization of the cell polarization [22]. Ohmic, activation, and concentration polarizations are related to electrical conductivity, triple phase boundary, and porosity, respectively. The volume percentage (vol%) of pores is an important parameter. Additionally, factors such as proper connectivity (open/close) pores, pore size and size distribution, and pore tortuosity play dominant roles in impacting polarization characteristics.

The porosity is often provided by pore-formers (such as graphitic carbon, short carbon fibers, polymer spheres, flour, rice, starch, etc.) in addition to the pore generated by NiO to Ni reduction [22]. In general, larger pore-formers (~20 µm) are more effective than small ones (a few microns) [22]. A certain vol% of pore-formers is necessary to generate a

network of open percolated pores, which is often ~30 vol%. It has also been suggested that composite pore-formers containing two or more pore-formers with different size ranges can be used to augment the pore network connectivity and tailor the shrinkage kinetics [22]. Other methods, such as freeze-casting, can also be used to generate pores. In freeze-casting, pores are generated as a result of ice sublimation in aqueous slurries [23]. Figure 3 shows side-view schematic of the multilayer structure in a SOEC/SOFC. The corresponding materials, morphology, and other attributes of each layer are given in the right column.

Functional layers in SOECs and SOFCs (multi-materials and multi-layer devices)		
Material system	Morphology	Attributes
Oxygen Electrode	Porous (open pores)	Ionic/electronic conductivity, high catalytic activity, 10 – 50 μm
Buffer layer	Porous	Ionic/electronic conductivity, 0.1 – 5 μm
Solid Electrolyte	Dense	Ionic conductor, low electronic conductivity, 10 – 50 μm , sintering temperature 1300 – 1500 $^{\circ}\text{C}$
Functional Layer	Porous	Ionic/electronic conductivity, 0.1 – 5 μm
Fuel Electrode	Porous (open pores)	Ionic/electronic conductor, > 100 μm



40 μm

Figure 3. Side-view schematic of the multilayer structure in a SOEC/SOFC (left). The corresponding materials, morphology, and other attributes of each layer (right).

The interconnect is a layer that sits between each individual cell and connects them in series. Interconnects are exposed to both oxidizing and reducing sides of the cell at high temperatures and, therefore, have the most demanding material requirements among other cell components in terms of stability. Generally, in these devices, two types of interconnects are used, metallic and ceramic oxides [24]. Ceramics are more stable (particularly for long-term stability) under oxidizing environments; however, they have lower electrical conductivity compared to metals and are expensive. Metallic interconnects have a lower cost and higher electrical conductivity; however, they have less stability than ceramics at high temperatures. One approach to increase the stability of metallic interconnects is coating them with protective ceramic layers, including oxides, perovskites, and spinel. The most common ceramics for interconnect applications include lanthanum and yttrium chromites (YCrO_3 and LaCrO_3) and perovskite p-type semiconductors [24]. AM processes on these particular ceramics are very limited. The main challenge with these materials has been difficulty in sintering Cr-containing oxides due to the vaporization of Cr-O species that complicates the sintering process.

Ferritic stainless steels (FSSs) are good candidates among metals, given their low cost, favorable CTE, ease of manufacturing, and formation of high electrical conductivity oxides on their surface. Chromium (Cr) evaporation under high operation temperature, however, has been a major limiting factor. Formation of native chromium oxide, which increases the ohmic resistance, and chromium poisoning of the SOFC cathode are two major degradation mechanisms in these devices [24]. Metal-ceramic composites (cermets) are also under consideration for interconnects, given their thermal stability at high temperatures and good electrical conductivity.

Sealant is another important component in these devices, for which no AM process has been yet reported. Often, the maximum working temperature of these devices is determined by the glass transition temperature of the sealant. Gas-tight (hermetic) sealants provide electrical insulation (prevent short-circuiting) and prevent mixing of the fuel and the oxidant. Glass-ceramic sealants are low-cost and have acceptable performance and stability (in both reducing and oxidizing environments) [25]. Thermal attributes of sealants, including CTE, glass transition temperature, crystallization temperature, and melting point,

are the defining parameters for choosing a sealant. Glass-ceramic sealants form chemical bonding with the adjoining components and hence do not require external load during operation. These sealants provide low cost and reasonable stability, as well as flexible design by varying the composition. Partial crystallization by sintering above the device's operating temperature can be achieved, which results in hermetic sealings. Currently, glass ceramics are fabricated by rolling, casting, pressing, and spin casting, among other methods. Both sealants and interconnects can be made of ceramic materials. As such, it is possible to develop AM processes based on full ceramics and cermets.

3. Reports in the Literature on Additive Manufacturing of SOFCs and SOECs

Several AM processes have been used for 3D printing of these devices, although mostly for a partial device [13,16]. These methods include inkjet printing (IJP) [11,26–41], stereolithography (SL) [8,42], and digital light processing (DLP) [18,43], with inkjet printing currently being the prevalent method. However, perhaps other than printing corrugated surfaces, so far, the printed cells and functional layers have all been planar, and no advanced 3-dimensional configurations to potentially gain higher specific power have been reported, yet. We also note that most of the reports have been on SOFCs. However, considering that these devices are very similar in structure and operation, processes can be applied to printing SOECs.

3.1. Inkjet Printing

Inkjet printing of SOFC components has been widely reported in the literature. The first report on inkjet printing of fuel cells dates back to 2008, in which the authors printed a NiO-YSZ interlayer and a YSZ electrolyte layer (both ~6 μm thick) on commercial NiO-YSZ anode support [44]. Since then, various components of SOFCs have been printed using inkjet printing, including electrolyte [29,40,41,44], anode micro-pillars [45], oxide cathode and composite cathode [28,32–34], intermediate cathode layer [35], cathode, interlayers, and electrolyte [30], anode and electrolyte [36], and even an entire SOFC [26]. It has been demonstrated that inkjet printing can be used to produce complete SOFCs with an electrochemical performance consistent with traditional processing methodologies [30]. Electrolyte layers with a thickness in the sub-micron [26] to several microns range have been reported. Most inkjet-printed cells were anode-supported [26,44,45]. Often other layers are added using traditional manufacturing processes such as screen printing or brush coating. In addition to printing the structure, inkjet printing has also been used to inject or infiltrate other chemicals (such as yttrium-doped barium zirconate) into porous electrodes [31].

Farandos et al. printed micro-pillar arrays and square lattices with an optimized ink composition, and minimum feature size of 35 μm was achieved in sintered structures [29]. Han et al. used a commercial low-cost office printer (HP inkjet printer) to print an entire anode-supported SOFC with a sub-micron thin YSZ electrolyte [26]. To synthesize the ink, the authors used ceramics with particle size distribution in the range of 0.15–0.19 μm , smaller than the printer nozzle diameter [26]. The printed SOFC maintained high open circuit voltage and robust uniform microstructure during the electrochemical performance and, in the durability test, achieved a power output of 730 $\text{mW}\cdot\text{cm}^{-2}$ at 650 $^{\circ}\text{C}$ and a low degradation rate of 0.2 $\text{mV}\cdot\text{h}^{-1}$.

In 2022, Jang and Kelsall reported printing 3D NiO-YSZ structures using inkjet printing for enhanced performance of SOFCs [45]. Specifically, pillars with a 50 μm diameter and 100 μm inter-pillar spacing were printed using a custom-made NiO-YSZ ink. A pillar height of ~28 μm was obtained for 90-layer printing. The authors initially prepared porous NiO-YSZ support pellets by mixing powders with graphitized carbon black pore-formers and pressing them into pellets, and heating them to 800 $^{\circ}\text{C}$. Afterward, NiO-YSZ pillar-structured layer was printed on the support using an inkjet printer, followed by coating the surface of the pillars with YSZ electrolyte by dip-coating. Smaller particle sizes compared to the substrate were used to prevent nozzle clogging, and no pore-formers were used. The

YSZ electrolyte was sintered at 1450 °C for 5 h. The cell was completed by brush-coating LSM-YSZ ink on the surface of the sintered YSZ, followed by heat treatment at 1000 °C for 2 h [45].

The authors claimed that in NiO-YSZ pillar structures, the increased power density would not only result from the larger electrode/electrolyte interfacial area but also from extended TPB lengths in the Ni-YSZ pillars. Since the inkjet-printed NiO-YSZ pillars did not have pore-formers, the porosity in the pillars only originated from the volume decrease associated with NiO to Ni reduction, which is smaller than the porosity in the substrate originated from pore-formers. This lower porosity in the pillars can decrease the gas permeability, particularly for tall pillars with small diameters. Hence, the optimal height of pillars needs to be identified [45].

Huang et al. reported printing microtubular SOFCs using inkjet printing [46]. The anode (NiO-YSZ), electrolyte (YSZ), and cathode layers were all printed by inkjet onto a cylindrical ceramic substrate. Based on cross-section SEM images, the thickness of the cathode and anode was less than 30 µm. The 3D-printed cell achieved more than 4000 h of long-term operation at a constant current of 18.5 A and performed more than 1000 cycles of rapid thermal cycling without cell failure [46].

Inkjet printing is compatible with metal, polymer, ceramic, and composite inks. It requires relatively low-cost equipment, and conventional office printers can be modified to use for this purpose. The most important fabrication process aspects include ink formulation of active materials, inkjet deposition, printing optimization, and characterization of inkjet-printed thin films. These parameters overall affect the electrochemical performance of the printed cells. Inkjet printing requires a “printable” ink, which entails certain rheological properties. Suitable dispersants should be used to obtain “stable” inks to prevent sedimentation and particle agglomeration, which may result in clogged nozzles [37]. The particle size should be also much smaller than the nozzle diameter. This may require synthesizing customized inks [47].

SOFC and SOEC devices printed by inkjet printing may achieve lower operation temperatures since the printed electrodes and electrolytes can be thin films (a few microns down to submicron), which reduce ion transport energy loss. In principle, inkjet is scalable to large-area manufacturing since the substrate can be moved under the nozzle, in addition to the nozzle motion. For example, with proper design, inkjet printers may be integrated with roll-to-roll processes.

If inkjet printing is used to print several functional layers, given different sintering temperatures, not all layers can be sintered at one step, and often multi-step sintering is used. For example, in a study the anode/anode interlayer/electrolyte structure was co-fired at 1400 °C for 2 h, and after printing the cathode and cathode interlayer the cell was again sintered at 1200 °C for 1 h [30]. Along the same line, novel designs to achieve monolithic fuel cell stacks that require only a single heat treatment during manufacturing are promising [48].

The ink in the inkjet printer has low viscosity; hence, it has low solids loading. It has been claimed that thermal inkjet printing (as opposed to the more conventional piezoelectric inkjet printing) can operate with higher solids loading inks, which would increase print efficiency [38]. In inkjet printing, the required porosity for electrodes can be obtained by controlling the print density through “grey scale” adjustment in the digital print file [32]. In order to fabricate the microstructure-controlled LSCF cathodes with controlled porosity and thickness, Han et al. adjusted the grayscale of a black-and-white drawing in the software with luminosity or “brightness” values from 0 (black) to 255 (white) [32]. A similar approach can be used in a multi-cartridge printer to fabricate composite cathodes with a controlled composition [33]. Specifically, to print LSCF/GDC composite, the content and porosity of the LSCF and GDC layers were adjusted by controlling the color level in the printed images and the number of printing cycles [33]. The authors concluded that an optimum amount of GDC in the composite cathode improves the oxygen reduction rate. Similarly, inkjet printing of composite cathode (LSCF-GDC) has also been reported. The

composition and microstructure of the composite cathode were controlled by adjusting the proportions of source materials in ink and by varying the printing parameters [33].

To print SOECs and SOFCs, inkjet printing has, however, inherent limitations. The process is limited to thin films (hence planar designs), and special designs are required to obtain non-planar surfaces. It should be mentioned that micro-pillar-type geometry has been obtained using this process [29,45]. For example, a pillar height of $\sim 28 \mu\text{m}$ was obtained by 90-layer printing [45]. Obtaining thicker samples as the support would require many print layers and hence is time-consuming. Substrate wetting and film solidification become important for printing multilayers and should be considered in the process design. Organic solvents are used in certain inks, which may not be desirable [11]. Although, there has been a good number of reports that used water-based inks [29,40,41].

3.2. Aerosol Jet Printing

Aerosol Jet Printing (AJP) has also been used to print components of SOFCs. This is a more involved and costly piece of equipment compared to an inkjet printer. Sukeshini et al. have reported the deposition of YSZ electrolyte and functionally graded anode interlayers with compositional variation by AJP using ink suspensions of NiO and YSZ [27]. The dual atomizer configuration of the system allowed for on-demand material mixing to deposit a graded composite anode interlayer. For the composite anode layer, the authors prepared two separate inks using YSZ and NiO powders, solvents, dispersants, binders, and plasticizers, with solid loading of $\sim 35 \text{ wt.}\%$. A compositionally graded composite of NiO-YSZ was deposited on a YSZ substrate and sintered at $1400 \text{ }^\circ\text{C}$. Hand-pasted LSM, sintered at $1200 \text{ }^\circ\text{C}$, was used as the cathode layer to complete the cell [27]. Before electrochemical characterization, the anode side was reduced in 5% hydrogen in argon for a few hours. Reduced ohmic resistance and better electrochemical performance are expected by grading the anode such that a larger volume fraction of YSZ relative to Ni exists in the regions adjacent to the electrolyte, which, according to the authors, is achievable with further optimization [27].

3.3. Lithography-Based Printing (DLP and SL)

DLP and SL have the advantage of good surface quality and dimensional precision. The resolution of a DLP printer is generally $\sim 50 \mu\text{m}$ in-plane (XY-plane) [18], with a layer thickness of $25 \mu\text{m}$ [18] to $50 \mu\text{m}$ [43]. Herein lies the significant challenge for printing SOECs and SOFCs, which is obtaining thin electrolyte layers ($\sim 5\text{--}10 \mu\text{m}$) using lithography-based printers since several layers are often required to obtain a structure with reasonable mechanical properties. Hence, these processes (DLP and SL) would not be suitable if achieving thin electrolytes (and hence lower ionic loss) is desirable. Consequently, current reports on lithography-based printing of these devices are all electrolyte-supported with a thick electrolyte layer [8,18,42,43]. The thickness of printed electrolytes in these reports varies from $200 \mu\text{m}$ to $500 \mu\text{m}$ [8,18,42,43].

If DLP and SL processes are used to only print a component of the cell (often the electrolyte), the anode and cathode are added by conventional means, including brush painting, spraying, etc., followed by heat treatment (or annealing), which is often at a higher temperature for NiO-YSZ than for LSM-YSZ [8,18,42,43]. For example, NiO-8YSZ slurry and LSM slurry were applied to the surface of the as-sintered 8YSZ electrolyte layer by brush painting. The NiO-8YSZ slurry and LSM slurry were prepared using their corresponding commercial powders [18]. Wei et al. sprayed cermets consisting of Ag and GDC as the materials of anode and cathode on printed electrolyte [43]. After application, the anode and cathode materials were annealed. In another report, commercial NiO-YSZ and LSM-YSZ paste were painted on a 3D-printed YSZ electrolyte as fuel and oxygen electrodes, respectively, followed up by thermal treatment at $1400 \text{ }^\circ\text{C}$ (3 h) and $1200 \text{ }^\circ\text{C}$ (1 h), respectively [8]. In this work, $250 \mu\text{m}$ -thick 8YSZ electrolyte-supported SOFCs with conventional planar and high-aspect ratio corrugated electrolytes were printed using the SL process [8]. Cells with corrugated layers showed an increase of 57% in their performance

in the fuel cell and co-electrolysis (of CO₂ and steam) modes in the temperature range of 800–900 °C. This enhancement was attributed to the larger area (~60%) compared to the cells with planar layers. The printed cells showed a degradation rate of 0.035 mV h⁻¹ [8]. In another electrolyte-supported design, authors printed honeycomb geometry cells consisting of 260 µm-thick hexagonal cells forming a network connected by 530 µm-thick beams of 220 µm in width. A simulation study confirmed that the honeycomb structure enhanced the cell performance compared to the flat counterpart. The authors speculated that this was because of enabling a thinner membrane and partly using the area increase associated with the beams [42].

To achieve the desired densification and prevent warpage, crack formation, and delamination during shrinkage in debinding and sintering in lithography-based printing, high solids loading (>30–60%) and stable and uniform photocurable slurries are required [18,43]. Successful sintering and debinding additionally requires optimization of thermogravimetric properties of the binder, which is nontrivial for multilayers and multi-materials in SOECs and SOFCs. Generally, a viscosity <5–20 Pa at a shear rate of 30 s⁻¹ is recommended for a photocurable resin [49], which makes using highly-loaded resins challenging. Heating the vat during printing can be used to lower the viscosity. To a certain degree, the addition of several particle sizes in the slurry can help achieve high solids loading while maintaining low viscosity [43].

Noticeable interfaces from layer-by-layer printing may compromise the mechanical and electrical properties of the printed ceramic (and cermet) layers and affect the electrochemical performance of the cell. Xing et al. obtained a smaller power density for electrolytes printed by DLP compared to cells with similar electrolyte thickness, which the authors attributed mainly to the layer boundaries between the printed 50 µm thick layers in the DLP process, in addition to the separation of the cathode layer from the electrolyte [18]. This is despite an OCV of ~1.1 obtained for the cells, which is more indicative of the gas tightness of the printed electrolyte.

It is not clear if DLP or SL processes are capable of printing porous electrodes. A possible method to obtain porous parts would be adding pore-formers to the photocurable resin. However, the addition of pore-formers may result in the diffraction of light and compromised geometrical tolerance or even partial curing. Pores can also be obtained by partial sintering, which is not desirable due to compromised mechanical properties. The reduction of NiO to Ni is associated with a 40% volume reduction [22]. Therefore, depending on the amount of NiO, small pores (either open or closed) (<1–3 µm) can be obtained by NiO to Ni reduction.

It should be noted that electrodes (cathode and anode) can also be printed first and then impregnated [17]. In this scenario, the ceramic phase of the cermet is 3D-printed (for example, the YSZ phase in NiO-YSZ) and then impregnated (infiltrated) with the corresponding metal phase. Generally, there are three impregnation methods, which include metal-salt solutions with various additives, impregnation with nanoparticles in a suspension, and molten salt impregnation [17]. Impregnation, in fact, has certain advantages since the catalytic phases are not sintered under the high temperatures required for sintering ceramic phases. They can be simply fired and dried under lower temperatures. This lower processing temperature and the small catalyst particle sizes can potentially prevent Ni migration and coarsening and complex microstructural evolution.

3.4. Robocasting

Robocasting (or direct ink writing) process is essentially compatible with any materials and pore-formers [5]. However, the resolution of this process is comparatively low. Additionally, achieving thin electrolytes in the range of several microns by robocasting would be nontrivial. As such, this method will need to be combined with other methods in a hybrid process to print a full cell. Anelli et al. reported symmetrical cells with the composition LSM-YSZ/YSZ/LSM-YSZ by a robocasting and inkjet printing hybrid technology, followed by a co-sintering step [50]. The LSM-YSZ electrodes were printed by robocasting by adding

pore-formers, while the water-based YSZ ink was printed using inkjet printing. After printing all layers, co-sintering of the fully printed cell was carried out at 1200 °C for 1 h in air. The final sintered electrolyte had a thickness of ~2.8 μm. For this cell, the electrochemical characterization led to an area-specific resistance (ASR) value of ~2.1 Ω cm² at 750 °C.

3.5. Other Potentially Applicable Processes

There are other AM processes that have the potential to contribute to the fabrication of these electrochemical devices. For example, the layer-wise nature of these devices is compatible with the laminated object manufacturing (LOM) process [51]. However, currently, the relevant scales are not compatible. Perhaps a process such as LOM with the possibility of achieving thinner laminates can be a useful process to be developed. Laser processing of ceramic materials can be potentially applicable to these devices, more for surface modification for patterning or subtractive processes such as drilling and machining [52].

Table 1 provides a comparison of the two main AM processes for printing SOECs and SOFCs. The first column lists the advantages of each printing process. The second column provides the limitations of each process in printing SOFCs and SOECs. The third column adds other considerations that must be considered when each process is used for printing these devices. Table 2 provides a summary of the reported work in the literature.

Table 1. Comparison of the two main AM processes for printing SOECs and SOFCs.

Printing Process	Advantages	Limitations	Considerations
Inkjet	<ul style="list-style-type: none"> - Compatible with thin films (sub-μm to several μm) - Possible to design aqueous inks (to reduce use of organic solvents) - Compatible with metal, polymer, ceramic and composite inks - Scalable to large areas - Control of porosity through “grey scale” adjustment 	<ul style="list-style-type: none"> - Mostly limited to planar geometries - Low solids loading inks, hence prone to delamination and warping during sintering - Limitation in particle size << nozzle diameter - Limited surface quality - Limited dimensional precision 	<ul style="list-style-type: none"> - Substrate wetting - Film solidification - Co-sintering - Organic solvents - Ink stability
Lithography based (SL and DLP)	<ul style="list-style-type: none"> - Good surface quality - Good dimensional precision - Compatible with 3D design and geometries - Compatible with high solids loading slurries 	<ul style="list-style-type: none"> - Print thickness of >25–50 μm, not suitable for thin electrolytes - Lengthy debinding (hours to days), resulting in high cost - Not compatible with multi-materials - Handling pore-formers to obtain porous structures 	<ul style="list-style-type: none"> - Low slurry viscosity requirement for printing while desiring high solids loading - Slurry rheology and stability - Interfacial properties

Table 2. A summary of reported work in the literature.

Printed Component	Printing Method	Notes	Reference
NiO-YSZ interlayer and YSZ electrolyte layer	Inkjet	Both layers were ~6 μm thick. Sintering temperature 1375–1400 °C. Open circuit voltages ranged from 0.95 to 1.06 V, and a maximum power density of 0.175 W·cm ⁻² was achieved at 750 °C.	[44]
Entire anode-supported cell	Inkjet	Achieved power output of 730 mW·cm ⁻² at 650 °C and a low degradation rate of 0.2 mV·h ⁻¹ .	[26]
YSZ electrolyte and Micro-pillar anode	Inkjet	A pillar height of ~28 μm was obtained for 90-layer printing. YSZ electrolyte was sintered at 1450 °C.	[45]

Table 2. Cont.

Printed Component	Printing Method	Notes	Reference
YSZ electrolyte and YSZ-LSM electrode	Inkjet	YSZ electrolyte and YSZ-LSM electrode were 9 and 20 μm thick, respectively. At 788 $^{\circ}\text{C}$, the peak fuel cell power density was $0.69 \text{ W}\cdot\text{cm}^{-2}$, and at a cell potential difference of 1.5 V.	[28]
Microtubular cells (anode (NiO-YSZ), electrolyte (YSZ) and cathode layers)	Inkjet	More than 4000 h of long-term operation at a constant current of 18.5 A and at 788 $^{\circ}\text{C}$, the peak fuel cell power density was 0.69 W cm^{-2} , and at a cell potential difference of 1.5 V.	[46]
YSZ electrolyte	Inkjet	23 mm thick planar electrolyte. A current density of -0.78 A cm^{-2} was obtained. Sintered at 1500 $^{\circ}\text{C}$.	[29]
YSZ electrolyte	Inkjet	150 nm films were obtained.	[40]
YSZ electrolyte	Inkjet	1.2 μm film was obtained. Peak power density above $1.5 \text{ W}\cdot\text{cm}^{-2}$ at 800 $^{\circ}\text{C}$ was obtained. Sintered at 1300 $^{\circ}\text{C}$.	[41]
YSZ electrolyte	Inkjet	Power density of $170 \text{ mW}\cdot\text{cm}^{-2}$ at 800 $^{\circ}\text{C}$ was obtained.	[39]
Electrolyte and buffering (SDC) layers	Inkjet (thermal)	Peak power density (PPD) of $860 \text{ mW}\cdot\text{cm}^{-2}$ at 800 $^{\circ}\text{C}$. Sintered at 1400 $^{\circ}\text{C}$.	[38]
NiO anode	Inkjet	Calcinated in air at 900 $^{\circ}\text{C}$.	[47]
Nio-YSZ	Inkjet	Sintered at 1295 $^{\circ}\text{C}$.	[37]
Anode interlayer and electrolyte	Inkjet	Sintered at 1400 $^{\circ}\text{C}$. Open circuit voltage of 1.1 V around 800 $^{\circ}\text{C}$. A maximum power density of $500 \text{ mW}\cdot\text{cm}^{-2}$ was achieved at 850 $^{\circ}\text{C}$.	[36]
LSCF-GDC composite cathode	Inkjet	Power output of over 570 mW cm^{-2} at 650 $^{\circ}\text{C}$ was obtained. Sintered at 950 $^{\circ}\text{C}$.	[33]
Intermediate cathode layer	Inkjet	Maximum power density of $0.71 \text{ W}/\text{cm}^2$ at 600 $^{\circ}\text{C}$ was obtained. Sintered at 1000 $^{\circ}\text{C}$.	[35]
YSZ pillar electrolyte	Inkjet (hybrid with tape casting)	Sintered at 1200 $^{\circ}\text{C}$.	[53]
Composite cathode	Inkjet	PPD as high as 940 mW cm^{-2} at 750 $^{\circ}\text{C}$ was obtained. Calcined at 1000 $^{\circ}\text{C}$.	[34]
Nio-YSZ anode layer, YSZ electrolyte and LSM cathode layer	Inkjet	An open-circuit voltage of 1.1 V and a maximum power density of $430\text{--}460 \text{ mW}/\text{cm}^2$ at 850 $^{\circ}\text{C}$ was obtained. Sintered at 1200 $^{\circ}\text{C}$.	[30]
LSCF cathode	Inkjet	A maximum peak power density of 377 mW cm^{-2} at 600 $^{\circ}\text{C}$ was obtained. Sintered at 950 $^{\circ}\text{C}$.	[32]
Ni-YSZ anode	Inkjet	Sintered at 1400 $^{\circ}\text{C}$. Anode with distribution-controlled Yttrium-doped Barium Zirconate.	[31]
Electrolyte and symmetric electrodes	Hybrid inkjet and robocasting	YSZ electrolyte by inkjet and LSM-YSZ symmetric electrodes by robocasting.	[50]
YSZ electrolyte and functionally graded anode interlayers	Aerosol Jet Printing	Graded composite anode interlayer was obtained. Anode interlayer was sintered at 1400 $^{\circ}\text{C}$.	[27]
YSZ electrolyte	DLP	An open circuit voltage of approximately 1.04 V and a peak power density up to 176 mW cm^{-2} at 850 $^{\circ}\text{C}$ was obtained. Sintered at 1550 $^{\circ}\text{C}$.	[43]

Table 2. Cont.

Printed Component	Printing Method	Notes	Reference
YSZ electrolyte	DLP	Sintered at 1450 °C.	[42]
YSZ electrolyte (corrugated surface)	DLP	Sintered at 1300 °C.	[8]
YSZ electrolyte	DLP	Sintered at 1450 °C.	[18]

4. Opportunities and Challenges for AM Technologies

Considering the reported AM work in the literature, limitations of the current manufacturing technologies and several challenges that must be overcome for AM to be a viable path for the manufacturing of SOECs and SOFCs are outlined below. Corresponding recommendations are provided to facilitate such efforts.

1. Eliminate or reduce stacking and lamination steps and enhance durability: Current AM technologies can print individual components such as the electrolyte or anode/cathode, and in some cases, several of the components such as anode and electrolyte. However, to compete with traditional manufacturing technologies for SOECs and SOFCs market, AM technologies should eliminate or reduce the stacking steps and/or enable continuous printing of integrated layers at the cell level and/or stack level, something that remains a formidable challenge [43]. Reducing the number of parts and interfaces will result in minimizing degradation and failure opportunities in these devices. Another point of view may be using AM only for components that are suitable for 3D printing rather than printing integrated cells and stacks. In this approach, a combination of additive and traditional manufacturing methods may be used. Essentially, AM will be used only if it can deliver reliable component(s) with complex geometries that cannot be manufactured otherwise and when there is enough performance gain justification. An example would be printing the electrolyte using DLP/SL and adding the electrodes by spraying or brushing or printing the electrolyte using an inkjet printer on a cathode fabricated by a traditional route such as power consolidation.

The push toward lower-cost hydrogen should be achieved with a long-term consideration of durability and efficiency. Such efforts, particularly in relevance to AM technologies, demand a holistic approach integrating standardization of testing and characterization protocols (including accelerated stress tests, ASTs), identification of common degradation mechanisms (preferably over the entire device lifetime and under realistic operation conditions), and their mitigation strategies, and improving durability (at the cell and stack level) and overall efficiency. Reproducible and uniform manufacturing and performance for high-volume manufacturing is a requirement for quality assurance and quality control (QA/QC). Currently, there are no studies in the literature on the long-term performance, durability, and degradation mechanisms of 3D-printed SOECs and SOFCs.

2. Facilitate co-sintering: Heat treatment comprises ~40% of the total manufacturing cost of these electrochemical devices (due to high temperature and long duration sintering and expensive equipment), and hence it is a major area for cost reduction [2]. This cost reduction is mostly through co-firing multiple layers. Several of the limitations or challenges of AM are common with traditional fabrication methods. An example is a requirement for co-sintering (co-firing) multiple layers of different materials (sometimes metals and ceramics) with different sintering temperatures and time requirements. The heating and cooling of such complex multilayer, multi-material parts is further complicated by the different CTE of adjacent layers. Continuous sintering (as opposed to batch furnaces) is considered a cost-reduction strategy. Similarly, microwave and plasma-assisted sintering are also considered viable cost-reduction strategies [54]. AM may enable denser and thinner layers, which will result in lower heat treatment time and cost, and more sample-to-sample uniformity. In addition to materials, another consideration in co-sintering is the influence of pore-formers on the shrinkage and sintering characteristics of electrodes [22].

Co-sintering is particularly attractive when electrodes are fabricated by catalyst infiltration into a porous ceramic scaffold since the interface between the ceramic electrolyte and the porous ceramic electrode will be strong, or no interface will be formed if the processing method can fabricate the porous electrode and dense electrolyte continuously. AM may also facilitate the manufacturing of functionally graded structures such that the transition from one material to another is optimized in terms of CTE.

3. Enable lower temperature operation: Potential AM technologies should also address the current push toward lower temperature operation (to ~500–600 °C or lower). Lower temperature operation is desirable to reduce or resolve some of the challenges, such as thermal management and the need for insulation, thermal stress, and the high degradation rate of current collectors and sealings. Lower operation temperatures may result in an increase in the device efficiency, as well as the possibility of using metals and polymers for these devices. This trend either requires thinner layers (using current materials) to reduce ionic/electronic resistance or the discovery of new low-temperature oxygen ion conductors. Additionally, microstructural variations such as columnar grains that have less resistance, substitutional doping, defect control, and fabrication of interfaces with less resistance (or elimination of interfaces in monolithically printed devices) may facilitate lower temperature operations.

The trend toward low temperature and thinner layers (tens of microns) will require printing technologies with better resolution. The thickness of each layer in the DLP/SL process is ~50 µm, while to reduce the resistance, a lower thickness electrolyte is required. One way to achieve thinner layers using AM is incorporating (printing) topologically optimized mechanical supports, for example, an electrolyte with thin and thick sections, which requires complex 3D designs [18].

4. Enable high-volume production and lower total cost: Ultimately, AM technologies will be compared to high-throughput processes such as roll-to-roll processes. Hence, cost analysis is a major factor in the success of AM technologies. For these electrochemical devices, materials and manufacturing costs are the major portion (~80%) of the total cost [2]. By increasing the number of units per year, the total manufacturing cost will significantly decrease. Currently, SOEC systems are not at cost-parity with conventional hydrogen production technologies (e.g., natural gas reforming) and will require technology development to achieve widespread deployment and commercialization. Likewise, SOFCs will require significant technological advancement to be cost-competitive with conventional combustion-based technologies currently used in stationary and vehicular applications. Without further development, these technologies are unlikely to economically support the predicted hydrogen market size.

There are three factors in the cost reduction of clean electrolytic H₂, namely electricity, capital cost, and fixed operations and maintenance. The current DOE goal is USD 2/kg by 2026 and USD 1/kg by 2031. The key enablers for lower-cost electrolytic H₂ include low-cost electricity, high electrical efficiency, low-cost capital expense, increased durability and lifetime, low-cost manufacturing processes, manufacturing at the MW scale, and increased power density. Analyses have projected a 4.5–6-time reduction in SOEC stack manufacturing cost through increasing manufacturing rates from 25 MW to 1 GW per year [2].

We should note that several manufacturing steps of 3D printing and traditional manufacturing are identical or similar depending on which process is used. These include slurry preparation (ball milling, rheological characterization), debinding (binder burnout), and (co)sintering. Accurate cost analysis for 3D printing technologies to produce SOECs and SOFCs requires consideration of the potential economies of scale. With the increase in demand, raw materials cost may reduce, and combined with enhanced device efficiency and durability, increased manufacturing throughput may result in an overall cost reduction and economic competency of 3D printing.

As an example, interconnects are often a major contributor to the total cost. Since interconnects are exposed to both oxidizing and reducing high-temperature environments,

ceramic materials can offer a stable and reliable option, albeit at a steep price. Metal-based interconnects will be more promising as lower temperature range (600–800 °C) devices are developed. Additive manufacturing can offer solutions for both metallic and ceramic interconnects, particularly for novel designs that incorporate optimized gas channels and better mechanical performance.

5. Enable complex geometries (beyond planar and tubular cells), different cell configurations and larger cell size: Currently, the most common geometries are planar and tubular geometries. Each of these designs has advantages/disadvantages in terms of volumetric efficiency, startup time, sealing quality and reliability, and manufacturing cost [55]. Modified planar designs enabled by AM may incorporate a wave-like (corrugated) structure or a micropillar-covered surface to increase the surface area. Additionally, AM may enable the incorporation of optimized gas flow channels within the cell structure to improve transport and ultimately result in higher power density. On the other hand, for more complex geometries, the dimensional changes during binder burnout and sintering become more challenging to predict and account for, which will require sophisticated modeling and simulation.

Generally, there are three configurations for each cell that includes electrolyte-supported, electrode-supported, and metal-supported, and each may have its own sub-categories [56,57]. For example, an anode-supported cell can be monolithic, in which the entire anode has the same morphology, or it can be a bi-layer, in which two different layers with different morphology and composition form the anode. In a bi-layer configuration, the thinner anode layer closer to the electrolyte is considered the anode functional layer (AFL). Similarly, the cathode functional layer (CFL) may be implemented on the cathode side. Being able to 3D print these functional layers with fine microstructure and optimized composition is expected to enhance the electrochemically active sites at the electrode/electrolyte interface and reduce contact resistance.

In metal-supported cells (MS-SOFCs), the Ni-YSZ electrode support is replaced with porous stainless steel, Ni, or other metals. The porous metal support is believed to improve strength (mitigate brittle failure associated with ceramics) and tolerance to aggressive operating conditions such as rapid thermal cycles, increase the redox tolerance and reduce the cost [57]. Currently, metal-supported cells are not as developed as anode-supported cells, and some aspects of degradation and oxidation issues need to be addressed. Given the much-developed AM technologies for metals, the development of metal-supported cells may benefit from 3D printing.

Larger cells require fewer stack materials and supporting infrastructure such as insulation, and hence result in higher power density. Therefore, increased cell size is considered a pathway for overall cost reduction. However, since the density of flaws increases with an increase in size, these mostly ceramic devices would suffer from lower strength for larger sizes (the Griffith theory of fracture mechanics). A similar concept may be applicable to having integrated channels into the 3D printed devices since they will change the entire stress field and stress concentration points, as well as electrochemical performance. Hence, mechanics and electrochemical performance analysis must be performed for various 3D printed designs.

6. Enable morphology (mostly pores) control: Porosity plays a significant role in cell and electrode polarization; hence, control and optimization of pore morphology is key to any manufacturing process. Traditional processing such as tape casting with pore-formers, provides limited control over pore morphology. Although an open-pore network is required, orientation and tortuosity of the pores deserve special attention. If the pores are aligned in the direction of the electrolyte/electrode interface, they are ineffective. Additionally, a tortuous path hinders gas diffusion. If AM can provide a type of porosity that is aligned perpendicular to the electrolyte/electrode interface (for example cylindrical), the generated porosity will effectively enhance gas diffusion. Creative channels and pores can be designed, for example, as the ones inspired by biological systems that optimize gas diffusion while maintaining mechanical integrity. We note that aspects of pore engineering

vary depending on the cell configuration. If the structural support in the cell is provided by an anode (anode-supported cells), the thickness of the anode needs to be higher (0.5–1.5 mm). With such a high thickness, engineering pore morphology becomes more important to prevent increased polarization [22].

7. Enable “true” multi-material, multi-scale 3D printing: The “multi-material printing” term has been used in various contexts in the literature [58], and it may need clarification to be accurate. A printer that can print one of the general family of materials (polymers, metals, or ceramics) in various forms and compositions may be called a multi-material printer. Examples may include a polymer printer that can print two different polymers with different stiffnesses, or colors, as in FDM (fused deposition modeling) printers; or a multi-nozzle printer that is connected to two or more reservoirs and can print each or combination of the inks by mixing and extrusion through the same nozzle such as in direct write-type printers; or a metal printer that can print alloys with different components such as in direct energy deposition printers.

The case for printing SOECs and SOFCs goes much beyond these points, and it can be argued that, currently, there is no such technology to satisfy all the requirements. A hypothetical multi-material, multi-scale printer to print these devices should be able to print ceramics (electrolyte), cermets (anode and cathode), and metals (contacts and interconnects), in addition to glass sealings. The printer should be able to print at multiple scales, as thin as a few microns (for electrolyte and anode/cathode functional layers) and several hundreds of microns (for example, for anode support). Currently, one inherent limitation of AM technologies is the generation of porous structures required for electrodes because these methods are not compatible with pore-formers (nozzle clogging in an inkjet printer and light scattering in DLP and SL). Therefore, the ideal printer should be able to adjust and control the porosity level (porous for anode and cathode and dense for electrolyte). Such requirements are nontrivial.

If manufacturing of complete SOFCs/SOECs is intended, SL and DLP have limitations in achieving multi-material printing capability. In order to print multi-materials in a DLP/SL type printer, multiple vats with different resin compositions (multiple exchanging resin vats) should be used [58]. In this method, the printing plate (platform) must be moved from one bath to another, with an additional step of washing and drying between each vat, which overall results in a slow and complex process, with possible contamination in between different vats and compromised materials composition and the possibility of low adhesion between interlayers of different materials [58]. Although inkjet printing is inherently compatible with different classes of materials, it is mostly limited to 2D geometries.

8. Enable robotic-assisted multi-printer process: Developing a printer that can print these devices is a monumental challenge. However, as it is common in the semiconductor industry, for a chip to be manufactured, multiple processes using multiple machines are involved. If such processes can be developed that are able to print various components of these devices in series, such a manufacturing process may be amenable to robotic and automation [59]. Given that a single printer is unlikely to print an entire cell or stack, robotic-assisted manufacturing may be relevant for SOFCs and SOECs. Robotic systems can transfer parts from one printer to the next to complete the process. Within the traditional manufacturing process, tape-casting, heat treatment, and stack assembly are considered the best candidates for automation. Therefore, this may raise the question of “what the advantages of such multi-process 3D printing would be compared to traditional manufacturing processes, i.e., automation of tape-casting, and stacking process?” A question that needs to be answered.

9. Incorporate computational design and modeling: Computational design may play a major role in efforts toward commercialization of these technologies, given the high cost of manufacturing and numerous iterations to find the optimal design with the most durable configuration and the lowest cost. AM should be combined with physics-based modeling and topology optimization to investigate the effects of complex 3D device geometries on

temperature distribution, flow velocity, pressure, and air and gaseous fuel concentrations through the cell and gas channels, and in turn, the effect of these parameters on the electric potential and current density distribution and performance of the device. Modeling of these devices often requires Multiphysics software platforms, including electrochemistry, fluid flow, heat transfer, and thermal and structural models. As an example, it is known that the gas channels in electrodes have a paramount effect on oxygen distribution and cell performance.

Table 3 provides a summary of the challenges and opportunities of AM of SOECs and SOFCs.

Table 3. Challenges and opportunities of AM of SOECs and SOFCs.

Challenges	Opportunities
1. Eliminate or reduce stacking and lamination steps and enhance durability	<ul style="list-style-type: none"> - Enable continuous printing of integrated layers. - Reduce the number of parts and interfaces - Integrate standardization of testing protocols (including accelerated stress tests), identification of common degradation mechanisms and their mitigation strategies. - Implement quality assurance and quality control (QA/QC) for AM devices.
2. Facilitate co-sintering	<ul style="list-style-type: none"> - Co-sintering of complex multilayer, multi-material parts having different CTE. - Fabricate parts that are amenable to continuous, microwave, or plasma-assisted sintering (thinner, topologically optimized for heat transfer, functionally graded structures, etc.)
3. Enable lower temperature operation	<ul style="list-style-type: none"> - Columnar grains, defect control, optimized interfaces. - Thinner layers through topologically optimized mechanical supports. - Complex 3D design.
4. Enable high-volume production and lower total cost	<ul style="list-style-type: none"> - Reduce number of manufacturing steps, automate the process. - Increase manufacturing rate to reduce price. - Enhanced device efficiency and durability. - Design and manufacture durable and optimized interconnects.
5. Enable complex geometries, different cell configurations and larger cell size	<ul style="list-style-type: none"> - Enable complex designs beyond planar and tubular. - Manufacture wave-like (corrugated) structures or micropillar-covered surfaces to increase surface area. - Integrate with modeling to account for dimensional changes during binder burn-out and sintering for complex 3D geometries. - Expand on metal-supported cell design. - Consider effects of increased size on the mechanics of ceramic components.
6. Enable morphology (mostly pores) control	<ul style="list-style-type: none"> - Provide control over orientation and tortuosity of the pores (non-tortuous pores perpendicular to the electrolyte/electrode interface). - Pore designs optimized for gas diffusion (for example bioinspired).
7. Enable “true” multi-material, multiscale 3D printing	<ul style="list-style-type: none"> - Enable printing ceramics (electrolyte), cermets (anode and cathode), metals (contacts and interconnects), and glass sealings. - Enable multiscale printing (a few microns for electrolyte) and tens-hundreds of microns for electrodes.
8. Enable robotic-assisted multi-printer process	<ul style="list-style-type: none"> - Develop processes based on several printers complemented with robotic and automation.
9. Incorporate computational design and modeling	<ul style="list-style-type: none"> - To find the optimal design, with the most durable configuration and the lowest cost. - Physics-based modeling and topology optimization to investigate effects of complex 3D device geometries on device performance.

5. Outlook

Overall, it can be argued that AM can provide a viable technological path for at-scale and low-cost manufacturing of SOECs and SOFCs, or thinking more conservatively, it can address several of the outstanding manufacturing issues. However, current AM technologies have major limitations for production of these complex devices, in terms of scale, time, cost, material compatibility, among others. It is expected that these issues will be resolved overtime as AM technologies become more matured and new AM technologies are developed. This endeavor will require investments from both the governments and the private sector to organize global collaborative efforts and initiatives.

Funding: This work is supported by the AESF foundation under the AESF Foundation Research Program and the US National Science Foundation (CMMI award number 2152732).

Institutional Review Board Statement: Not applicable.

Informed Consent Statement: Not applicable.

Conflicts of Interest: The authors declare no conflict of interest.

References

1. *Achieving American Leadership in the Hydrogen Supply Chain*; U.S. Department of Energy: Washington, DC, USA, 2022.
2. *High Temperature Electrolysis Manufacturing Workshop Summary Report, Hydrogen and Fuel Cell Technologies Office*; U.S. Department of Energy: Washington, DC, USA, 2022.
3. Hauch, A.; Küngas, R.; Blennow, P.; Hansen, A.B.; Hansen, J.B.; Mathiesen, B.V.; Mogensen, M.B. Recent advances in solid oxide cell technology for electrolysis. *Science* **2020**, *370*, eaba6118. [[CrossRef](#)] [[PubMed](#)]
4. *Water Electrolyzers and Fuel Cells Supply Chain: Supply Chain Deep Dive Assessment U.S. Department of Energy Response to Executive Order 14017, "America's Supply Chains"*; U.S. Department of Energy: Washington, DC, USA, 2022.
5. Cramer, C.L.; Ionescu, E.; Graczyk-Zajac, M.; Nelson, A.T.; Katoh, Y.; Haslam, J.J.; Wondraczek, L.; Aguirre, T.G.; LeBlanc, S.; Wang, H.; et al. Additive manufacturing of ceramic materials for energy applications: Road map and opportunities. *J. Eur. Ceram. Soc.* **2022**, *42*, 3049–3088. [[CrossRef](#)]
6. Ruiz-Morales, J.C.; Tarancón, A.; Canales-Vázquez, J.; Méndez-Ramos, J.; Hernández-Afonso, L.; Acosta-Mora, P.; Marín Rueda, J.R.; Fernández-González, R. Three dimensional printing of components and functional devices for energy and environmental applications. *Energy Environ. Sci.* **2017**, *10*, 846–859. [[CrossRef](#)]
7. Weimar, M.R.; Chick, L.A.; Gotthold, D.W.; Whyatt, G.A. *Cost Study for Manufacturing of Solid Oxide Fuel Cell Power Systems*; Contract DE-AC05-76RL01830; Pacific Northwest National Laboratory: Richland, WA, USA, 2013.
8. Pesce, A.; Hornés, A.; Núñez, M.; Morata, A.; Torrell, M.; Tarancón, A. 3D printing the next generation of enhanced solid oxide fuel and electrolysis cells. *J. Mater. Chem. A* **2020**, *8*, 16926–16932. [[CrossRef](#)]
9. Bertei, A.; Tariq, F.; Yufit, V.; Ruiz-Trejo, E.; Brandon, N.P. Guidelines for the Rational Design and Engineering of 3D Manufactured Solid Oxide Fuel Cell Composite Electrodes. *J. Electrochem. Soc.* **2016**, *164*, F89–F98. [[CrossRef](#)]
10. Chueh, C.-C.; Bertei, A. Thermo-mechanical analysis of 3D manufactured electrodes for solid oxide fuel cells. *J. Eur. Ceram. Soc.* **2021**, *41*, 497–508. [[CrossRef](#)]
11. Zouridi, L.; Garagounis, I.; Vourros, A.; Marnellos, G.E.; Binas, V. Advances in Inkjet-Printed Solid Oxide Fuel Cells. *Adv. Mater. Technol.* **2022**, *7*, 2101491. [[CrossRef](#)]
12. Deiner, L.J.; Reitz, T.L. Inkjet and Aerosol Jet Printing of Electrochemical Devices for Energy Conversion and Storage. *Adv. Eng. Mater.* **2017**, *19*, 1600878. [[CrossRef](#)]
13. Tai, X.Y.; Zhakeyev, A.; Wang, H.; Jiao, K.; Zhang, H.; Xuan, J. Accelerating Fuel Cell Development with Additive Manufacturing Technologies: State of the Art, Opportunities and Challenges. *Fuel Cells* **2019**, *19*, 636–650. [[CrossRef](#)]
14. Rasaki, S.A.; Liu, C.; Lao, C.; Zhang, H.; Chen, Z. The innovative contribution of additive manufacturing towards revolutionizing fuel cell fabrication for clean energy generation: A comprehensive review. *Renew. Sustain. Energy Rev.* **2021**, *148*, 111369. [[CrossRef](#)]
15. Zhang, X.; Wu, X.; Shi, J. Additive manufacturing of zirconia ceramics: A state-of-the-art review. *J. Mater. Res. Technol.* **2020**, *9*, 9029–9048. [[CrossRef](#)]
16. Ambrosi, A.; Shi, R.R.S.; Webster, R.D. 3D-printing for electrolytic processes and electrochemical flow systems. *J. Mater. Chem. A* **2020**, *8*, 21902–21929. [[CrossRef](#)]
17. Connor, P.A.; Yue, X.; Savaniu, C.D.; Price, R.; Triantafyllou, G.; Cassidy, M.; Kerherve, G.; Payne, D.J.; Maher, R.C.; Cohen, L.F.; et al. Tailoring SOFC Electrode Microstructures for Improved Performance. *Adv. Energy Mater.* **2018**, *8*, 1800120. [[CrossRef](#)]
18. Xing, B.; Cao, C.; Zhao, W.; Shen, M.; Wang, C.; Zhao, Z. Dense 8 mol% yttria-stabilized zirconia electrolyte by DLP stereolithography. *J. Eur. Ceram. Soc.* **2020**, *40*, 1418–1423. [[CrossRef](#)]

19. Shi, Y.; Cai, N.; Cao, T.; Zhang, J. *High-Temperature Electrochemical Energy Conversion and Storage: Fundamentals and Applications*; CRC Press: Boca Raton, FL, USA, 2018.
20. Liu, Y.; Shao, Z.; Mori, T.; Jiang, S.P. Development of nickel based cermet anode materials in solid oxide fuel cells—Now and future. *Mater. Rep. Energy* **2021**, *1*, 100003. [[CrossRef](#)]
21. Ferreira, V.J.; Wolff, D.; Hornés, A.; Morata, A.; Torrell, M.; Tarancón, A.; Corchero, C. 5 kW SOFC stack via 3D printing manufacturing: An evaluation of potential environmental benefits. *Appl. Energy* **2021**, *291*, 116803. [[CrossRef](#)]
22. Shri Prakash, B.; Senthil Kumar, S.; Aruna, S.T. Properties and development of Ni/YSZ as an anode material in solid oxide fuel cell: A review. *Renew. Sustain. Energy Rev.* **2014**, *36*, 149–179. [[CrossRef](#)]
23. Riyad, M.F.; Mahmoudi, M.; Minary-Jolandan, M. Manufacturing and Thermal Shock Characterization of Porous Yttria Stabilized Zirconia for Hydrogen Energy Systems. *Ceramics* **2022**, *5*, 472–483. [[CrossRef](#)]
24. Brouzgou, A.; Demin, A.; Tsiakaras, P. Interconnects for Solid Oxide Fuel Cells. In *Advances in Medium and High Temperature Solid Oxide Fuel Cell Technology*; Boaro, M., Salvatore, A.A., Eds.; Springer International Publishing: Cham, Switzerland, 2017.
25. Sulisty, G.; Iwan, S. Progress in Glass-Ceramic Seal for Solid Oxide Fuel Cell Technology. *J. Adv. Res. Fluid Mech. Therm. Sci.* **2021**, *82*, 39–50. [[CrossRef](#)]
26. Han, G.D.; Bae, K.; Kang, E.H.; Choi, H.J.; Shim, J.H. Inkjet Printing for Manufacturing Solid Oxide Fuel Cells. *ACS Energy Lett.* **2020**, *5*, 1586–1592. [[CrossRef](#)]
27. Sukeshini, A.M.; Meisenkothen, F.; Gardner, P.; Reitz, T.L. Aerosol Jet® Printing of functionally graded SOFC anode interlayer and microstructural investigation by low voltage scanning electron microscopy. *J. Power Sources* **2013**, *224*, 295–303. [[CrossRef](#)]
28. Farandos, N.M.; Li, T.; Kelsall, G.H. 3-D inkjet-printed solid oxide electrochemical reactors. II. LSM—YSZ electrodes. *Electrochim. Acta* **2018**, *270*, 264–273. [[CrossRef](#)]
29. Farandos, N.M.; Kleiminger, L.; Li, T.; Hankin, A.; Kelsall, G.H. Three-dimensional Inkjet Printed Solid Oxide Electrochemical Reactors. I. Yttria-stabilized Zirconia Electrolyte. *Electrochim. Acta* **2016**, *213*, 324–331. [[CrossRef](#)]
30. Sukeshini, A.M.; Cummins, R.; Reitz, T.L.; Miller, R.M. Inkjet Printing of Anode Supported SOFC: Comparison of Slurry Pasted Cathode and Printed Cathode. *Electrochem. Solid-State Lett.* **2009**, *12*, B176. [[CrossRef](#)]
31. Shimada, H.; Ohba, F.; Li, X.; Hagiwara, A.; Ihara, M. Electrochemical Behaviors of Nickel/Yttria-Stabilized Zirconia Anodes with Distribution Controlled Yttrium-Doped Barium Zirconate by Ink-jet Technique. *J. Electrochem. Soc.* **2012**, *159*, F360–F367. [[CrossRef](#)]
32. Han, G.D.; Neoh, K.C.; Bae, K.; Choi, H.J.; Park, S.W.; Son, J.-W.; Shim, J.H. Fabrication of lanthanum strontium cobalt ferrite (LSCF) cathodes for high performance solid oxide fuel cells using a low price commercial inkjet printer. *J. Power Sources* **2016**, *306*, 503–509. [[CrossRef](#)]
33. Han, G.D.; Choi, H.J.; Bae, K.; Choi, H.R.; Jang, D.Y.; Shim, J.H. Fabrication of Lanthanum Strontium Cobalt Ferrite–Gadolinium-Doped Ceria Composite Cathodes Using a Low-Price Inkjet Printer. *ACS Appl. Mater. Interfaces* **2017**, *9*, 39347–39356. [[CrossRef](#)]
34. Li, C.; Chen, H.; Shi, H.; Tade, M.O.; Shao, Z. Green fabrication of composite cathode with attractive performance for solid oxide fuel cells through facile inkjet printing. *J. Power Sources* **2015**, *273*, 465–471. [[CrossRef](#)]
35. Yashiro, N.; Usui, T.; Kikuta, K. Application of a thin intermediate cathode layer prepared by inkjet printing for SOFCs. *J. Eur. Ceram. Soc.* **2010**, *30*, 2093–2098. [[CrossRef](#)]
36. Sukeshini, M.A.; Cummins, R.; Reitz, T.L.; Miller, R.M. Ink-Jet Printing: A Versatile Method for Multilayer Solid Oxide Fuel Cells Fabrication. *J. Am. Ceram. Soc.* **2009**, *92*, 2913–2919. [[CrossRef](#)]
37. Rosa, M.; Zielke, P.; Kiebach, R.; Costa Bassetto, V.; Lesch, A.; Esposito, V. Printing of NiO-YSZ nanocomposites: From continuous synthesis to inkjet deposition. *J. Eur. Ceram. Soc.* **2019**, *39*, 1279–1286. [[CrossRef](#)]
38. Li, C.; Shi, H.; Ran, R.; Su, C.; Shao, Z. Thermal inkjet printing of thin-film electrolytes and buffering layers for solid oxide fuel cells with improved performance. *Int. J. Hydrogen Energy* **2013**, *38*, 9310–9319. [[CrossRef](#)]
39. Tomov, R.I.; Krauz, M.; Jewulski, J.; Hopkins, S.C.; Kluczowski, J.R.; Glowacka, D.M.; Glowacki, B.A. Direct ceramic inkjet printing of yttria-stabilized zirconia electrolyte layers for anode-supported solid oxide fuel cells. *J. Power Sources* **2010**, *195*, 7160–7167. [[CrossRef](#)]
40. Gadea, C.; Hanniet, Q.; Lesch, A.; Marani, D.; Jensen, S.H.; Esposito, V. Aqueous metal–organic solutions for YSZ thin film inkjet deposition. *J. Mater. Chem. C* **2017**, *5*, 6021–6029. [[CrossRef](#)]
41. Esposito, V.; Gadea, C.; Hjelm, J.; Marani, D.; Hu, Q.; Agersted, K.; Ramousse, S.; Jensen, S.H. Fabrication of thin yttria-stabilized-zirconia dense electrolyte layers by inkjet printing for high performing solid oxide fuel cells. *J. Power Sources* **2015**, *273*, 89–95. [[CrossRef](#)]
42. Masciandaro, S.; Torrell, M.; Leone, P.; Tarancón, A. Three-dimensional printed yttria-stabilized zirconia self-supported electrolytes for solid oxide fuel cell applications. *J. Eur. Ceram. Soc.* **2019**, *39*, 9–16. [[CrossRef](#)]
43. Wei, L.; Zhang, J.; Yu, F.; Zhang, W.; Meng, X.; Yang, N.; Liu, S. A novel fabrication of yttria-stabilized-zirconia dense electrolyte for solid oxide fuel cells by 3D printing technique. *Int. J. Hydrogen Energy* **2019**, *44*, 6182–6191. [[CrossRef](#)]
44. Young, D.; Sukeshini, A.M.; Cummins, R.; Xiao, H.; Rottmayer, M.; Reitz, T. Ink-jet printing of electrolyte and anode functional layer for solid oxide fuel cells. *J. Power Sources* **2008**, *184*, 191–196. [[CrossRef](#)]
45. Jang, I.; Kelsall, G.H. Fabrication of 3D NiO-YSZ structures for enhanced performance of solid oxide fuel cells and electrolyzers. *Electrochem. Commun.* **2022**, *137*, 107260. [[CrossRef](#)]

46. Huang, W.; Finnerty, C.; Sharp, R.; Wang, K.; Balili, B. High-Performance 3D Printed Microtubular Solid Oxide Fuel Cells. *Adv. Mater. Technol.* **2017**, *2*, 1600258. [[CrossRef](#)]
47. Sobolev, A.; Stein, P.; Borodianskiy, K. Synthesis and characterization of NiO colloidal ink solution for printing components of solid oxide fuel cells anodes. *Ceram. Int.* **2020**, *46*, 25260–25265. [[CrossRef](#)]
48. Pirou, S.; Talic, B.; Brodersen, K.; Hauch, A.; Frandsen, H.L.; Skafte, T.L.; Persson, Å.H.; Høgh, J.V.T.; Henriksen, H.; Navasa, M.; et al. Production of a monolithic fuel cell stack with high power density. *Nat. Commun.* **2022**, *13*, 1263. [[CrossRef](#)]
49. De Hazan, Y.; Heinecke, J.; Weber, A.; Graule, T. High solids loading ceramic colloidal dispersions in UV curable media via comb-polyelectrolyte surfactants. *J. Colloid Interface Sci.* **2009**, *337*, 66–74. [[CrossRef](#)] [[PubMed](#)]
50. Anelli, S.; Rosa, M.; Baiutti, F.; Torrell, M.; Esposito, V.; Tarancón, A. Hybrid-3D printing of symmetric solid oxide cells by inkjet printing and robocasting. *Addit. Manuf.* **2022**, *51*, 102636. [[CrossRef](#)]
51. Dermeik, B.; Travitzky, N. Laminated Object Manufacturing of Ceramic-Based Materials. *Adv. Eng. Mater.* **2020**, *22*, 2000256. [[CrossRef](#)]
52. Merino, R.I.; Laguna-Bercero, M.A.; Lahoz, R.; Larrea, Á.; Oliete, P.B.; Orera, A.; Peña, J.I.; Sanjuán, M.L.; Sola, D. Laser processing of ceramic materials for electrochemical and high temperature energy applications. *Boletín Soc. Española Cerámica Vidr.* **2022**, *61*, S19–S39. [[CrossRef](#)]
53. Salari, F.; Badihi Najafabadi, A.; Ghatee, M.; Golmohammad, M. Hybrid additive manufacturing of the modified electrolyte-electrode surface of planar solid oxide fuel cells. *Int. J. Appl. Ceram. Technol.* **2020**, *17*, 1554–1561. [[CrossRef](#)]
54. Bhattacharya, M.; Basak, T. A review on the susceptor assisted microwave processing of materials. *Energy* **2016**, *97*, 306–338. [[CrossRef](#)]
55. Singh, M.; Zappa, D.; Comini, E. Solid oxide fuel cell: Decade of progress, future perspectives and challenges. *Int. J. Hydrog. Energy* **2021**, *46*, 27643–27674. [[CrossRef](#)]
56. Tucker, M.C. Progress in metal-supported solid oxide fuel cells: A review. *J. Power Sources* **2010**, *195*, 4570–4582. [[CrossRef](#)]
57. Tucker, M.C. Progress in metal-supported solid oxide electrolysis cells: A review. *Int. J. Hydrogen Energy* **2020**, *45*, 24203–24218. [[CrossRef](#)]
58. Shaukat, U.; Rossegger, E.; Schlögl, S. A Review of Multi-Material 3D Printing of Functional Materials via Vat Photopolymerization. *Polymers* **2022**, *14*, 2449. [[CrossRef](#)] [[PubMed](#)]
59. MacDonald, E.; Wicker, R. Multiprocess 3D printing for increasing component functionality. *Science* **2016**, *353*, aaf2093. [[CrossRef](#)] [[PubMed](#)]